

Nano-Scale Particulate Matter from Urban Traffic
Rapidly Induces Oxidative Stress and Inflammation
in Olfactory Epithelium with Concomitant Effects on
Brain

Hank Cheng, Arian Saffari, Constantinos Sioutas,
Henry J. Forman, Todd E. Morgan, and Caleb E. Finch

<http://dx.doi.org/10.1289/EHP134>

Received: 16 September 2015

Revised: 29 February 2016

Accepted: 2 May 2016

Published: 17 May 2016

Note to readers with disabilities: *EHP* will provide a [508-conformant](#) version of this article upon final publication. If you require a 508-conformant version before then, please contact ehp508@niehs.nih.gov. Our staff will work with you to assess and meet your accessibility needs within 3 working days.

Nano-Scale Particulate Matter from Urban Traffic Rapidly Induces Oxidative Stress and Inflammation in Olfactory Epithelium with Concomitant Effects on Brain

Hank Cheng^{1,3}, Arian Saffari², Constantinos Sioutas², Henry J. Forman¹, Todd E. Morgan¹, and Caleb E. Finch^{1,3}

¹Davis School of Gerontology, ²Viterbi School of Engineering, ³USC Dornsife College, University of Southern California, Los Angeles, California, USA

Address correspondence to C.E. Finch, 3715 McClintock Ave, Gerontology-USC, Los Angeles, CA 90089-0191 USA. Telephone: 213 369 7600. E-mail: cefinch@usc.edu

Running title: Air pollution and inflammation in nose and brain

Acknowledgments: This work was supported by grants from the NIA (R21-AG040753, R21-AG040683, R01-AG051521) and the Southern California Children's Environmental Health Center grants: P30ES007048, P01ES022845, EPA83544101.

Competing financial interests: The authors declare no competing financial interests.

Abstract

Background: Rodent models for urban air pollution show consistent induction of inflammatory responses in major brain regions. However, the initial impact of air pollution particulate material on olfactory gateways has not been reported.

Objective: We evaluated the olfactory neuroepithelium (OE) and brain regional responses to a nano-sized subfraction of urban traffic ultrafine particulate matter (nPM, < 200 nm) in vivo, ex vivo and in vitro.

Methods: Adult mice were exposed to re-aerosolized nPM for 5-, 20-, and 45- cumulative hours (h) over 3 weeks. The OE, olfactory bulb (OB), cerebral cortex, and cerebellum were analyzed for oxidative stress and inflammatory responses. Acute responses of the OE to liquid nPM suspensions were studied with ex vivo and primary OE cultures.

Results: After exposure to nPM, the OE and OB had rapid increases of 4-hydroxy-2-nonenal (4-HNE) and 3-nitrotyrosine (3-NT) protein adducts, while cortex and cerebellum did not respond at any time. All brain regions showed increased tumor necrosis factor- α (TNF α) protein by 45 h, with earlier induction of TNF α mRNA in OE and OB. These responses corresponded to in vitro OE and mixed glial responses, with rapid induction of nitrite and inducible nitric oxide synthase (iNOS), followed by TNF α .

Conclusions: These findings show the differential time course of oxidative stress and inflammatory responses to nPM between the OE and the brain. Slow cumulative transport of inhaled nPM into the brain may contribute to delayed responses of proximal and distal brain regions, with potential input from systemic factors.

Introduction

The brain has emerged as a target of air pollution. Population based studies show cognitive impairments increase in proportion to levels of PM_{2.5} (Ailshire et al. 2014; Gatto et al. 2014; Tonne et al. 2014) and ozone, which approximate 3-5 years of accelerated cognitive loss (Chen and Schwartz 2009). Correspondingly, white matter loss was increased by 1% per 3 $\mu\text{g}/\text{m}^3$ PM_{2.5} in an MRI analysis of elderly women of the Women's Health Initiative Memory Study cohort (Chen et al. 2015). Cortical white matter volume changes and inflammation were also reported in a small sample of postmortem children from a highly polluted Mexican City (Calderón-Garcidueñas et al. 2011). Rodent models further document inflammatory responses of the cortex, olfactory bulb (OB), and midbrain to relatively short term exposure of automotive-derived air particulate matter (Campbell et al. 2005; Levesque et al. 2011a; Morgan et al. 2011; Block et al. 2012). Notably, TNF α induced by nano-sized particulate matter (nPM) can impair neurite outgrowth (Cheng et al. 2016).

We focus on the ultrafine class of PM (i.e. particles with diameter < 200 nm) to extend our prior studies (Morgan et al. 2011; Cheng et al. 2016). Additionally, ultrafine PM have higher in vivo and in vitro toxicity compared to larger PM derived from combustion engines (Li et al. 2002; Gillespie et al. 2013). Moreover, in inhalation studies, nano-sized particles could physically translocate to the OB and brain via the axons of olfactory sensory neurons in the OE, which project directly to synapses in the OB glomerulus (Oberdörster et al. 2004; Elder et al. 2006). These observations are supported by nasal instillation studies of ultrafine particles, which show translocation to the OB and induce TNF α and MIP1 α in OB (Wen-shwe et al. 2006). In vivo and in vitro, nPM induced IL-1 α , IL-6, and TNF α , with glial responses (CD68, GFAP) (Morgan et al. 2011; Cheng et al. 2016). Similarly, nano-scale diesel exhaust (DE) induced

TNF α , IL-6, MIP-1 α in olfactory bulb (OB) and post-olfactory brain regions (Levesque et al. 2011a). Thus, the OE may be an important gateway for the impact of ultrafine PM on the central nervous system.

While there are well-documented OE responses to ozone (Wagner et al. 2002; Ong et al. 2015), little is known about acute OE responses to acute air pollution PM in rodent models. Because the OE is the first neuronal contact to inhaled PM and because OE neuron dendrites regress with acute exposure in vitro to nPM (Cheng et al. 2016), we hypothesized that OE responses would be rapid and precede brain responses. We therefore defined the time course response of OE, OB, cerebral cortex, and cerebellum to nPM in vivo for oxidative stress (4-hydroxynonenal, 4-HNE and 3-nitrotyrosine, 3-NT) (Butterfield et al. 2011) and inflammatory responses (TNF α and microglia) (Kraft et al. 2011). Furthermore, we introduce an ex vivo model of the OE for studying acute responses to nPM. These exposure paradigms used a chemically defined nano-scale subfraction that we designated as nPM to distinguish it from the total ultrafine PM_{0.2 μ m} class (Morgan et al. 2011).

Material and Methods

nPM collection and extraction. Nano-scale particulate matter (nPM, <0.2 μ m in diameter) was collected on Teflon filters by a High-Volume Ultrafine Particle (HVUP) Sampler (Misra et al. 2002) at 400 L/min flow, about 150 meters downwind of the I-110 Freeway in central Los Angeles. nPM collected at this location between August and September 2012 represent urban ultrafine particles, dominantly originating from vehicular combustion emissions in addition to other less substantial sources such as sub-micron road dust (Hassheminassab et al. 2013; Saffari et al. 2013). The composition of collected nPM samples was similar to that of prior studies

(Morgan et al. 2011). Filter-trapped dried nPM were eluted by sonication into deionized water. nPM suspensions (150 µg/ml) were tested for sterility (no microbial growth in nutrient media) and stored at -20 °C. nPM slurries were endotoxin-free as assayed by Limulus assay (Davis et al. 2013). As controls for nPM extracts, fresh sterile filters were sham extracted. The slurries were then either re-aerosolized for animal exposure or used for treating cell cultures.

Animals and Ethics Statement. In vivo and ex vivo studies used 3-month old adult C57BL/6J male mice (body weight average: 27 g; n = 6/treatment/time, 36 total) purchased from Jackson Laboratories (Sacramento, CA, USA). Protocols were approved by the USC Institutional Animal Care & Use Committee (IACUC); animals were maintained following NIH guidelines. Mice were fed Purina Lab Chow (Newco, Rancho Cucamonga, CA) and sterile water *ad libitum*, and kept in standard animal housing facilities operated by USC Department of Animal Resources. Mice were housed in groups of 4 or 5 at 21-22 °C with 30% humidity, and kept in cages with standard bedding and nesting material that allowed for ample free movement. The light cycle time range was 06:00-18:00. For tissue collection, starting at 9AM, animals were euthanized by standard isoflurane, followed by cervical dislocation, and then perfused with saline. Organs were immediately frozen on dried ice after collection for storage. Animal procedures were performed at room temperature.

In vitro studies with primary cultures used pups from Sprague Dawley rats (received on pregnancy day 14) from Harlan Labs (Livermore, CA, USA). 3 pregnant rats were received for 3 experimental replicates and housed under standard conditions (Morgan et al. 2011). Pups were housed with the mothers prior to usage at postnatal day 3 (P3).

Exposure conditions. Mice were randomly assigned to groups, then exposed to nPM re-aerosolized by a HOPE nebulizer (B&B Medical Technologies) (Wang et al. 2013) at 343 $\mu\text{g}/\text{m}^3$ for 5 h (10AM-3PM)/day, 3 d (MWF)/week for cumulative 5, 20, or 45 h (see Supplemental Material, Fig. S1). The nPM slurry is dehydrated and charge-neutralized in the nebulizer chambers before mouse exposure. Particle number concentration of the inlet aerosol was monitored during exposures by a condensation particle counter (CPC, TSI Inc.) (Morgan et al. 2011; Wang et al. 2013). For exposure, mice were transferred from home cages into sealed exposure chambers that allowed adequate ventilation and with individual separation to minimize aggression. Exposed mice remained healthy and did not incur changes in body weight or core temperatures compared with controls measured prior to euthanasia (not shown).

Cell culture. For ex vivo OE organ cultures, adult mice were cardiac perfused with PBS (pH 7.4) and the nasal mucosa was delaminated as paired tissue ribbons (10 mg wet weight per mouse; 2 mice pooled per sample). The OE here is designated as the nasal mucosa lining the nasoturbinates and ethmoturbinates (Fig. 1A). OE were rinsed in PBS before 2 h incubation with 150 μl of nPM (12 $\mu\text{g}/\text{ml}$) diluted in artificial cerebral spinal fluid (aCSF: 119 mM NaCl, 26.2 mM NaHCO_3 , 2.5 mM KCl, 1 mM NaH_2PO_4 , 1.3 mM MgCl_2 , 10 mM glucose). Conditioned media (CM) were collected, centrifuged at 10,000g/5 min, and analyzed. Tissues were processed for RNA.

In vitro primary cell culture studies were originated from OE and mixed glia from cerebral cortex of P3 rats. The entire litter (both sexes) was used for primary cultures (~10 pups). For cell cultures, OE was dissociated via trituration and filtering using a 70 μm cell strainer. Cells were grown for 2 weeks in 6-well plates until 95% confluence, prior to addition of nPM for

nitrite time course (Griess assay). OE primary cell cultures at confluence contain mainly spindle-shaped cells (lacking GFAP, Iba1, and NeuN); a minority of cells (< 5%) expressed GFAP, Iba1, or NeuN (not shown).

For cerebral cortex mixed glia, cultures were grown for 2.5 weeks and comprised of 3:1 astrocytes: microglia, prior to treatment with trypsin for secondary cultures in 6-well plates. Secondary cultures were plated at approximately 1,000,000 cells/well. All primary cultures (OE, mixed glia) were grown in Dulbecco's modified Eagle's medium/Ham's F12 50/50 Mix (DMEM F12 50/50) supplemented with 10% fetal bovine serum (FBS), 1% Pen/Strep and 1% L-glutamine in a humidified incubator (37°C/5%CO₂) (Rozovsky et al. 1998). For treatment of cells, nPM (12 µg/ml) was diluted in Dulbecco's modified Eagle's medium (DMEM) supplemented with 15 mM HEPES, 1% sodium pyruvate, 0.24% BSA, 1% Pen/Strep, and 1% L-glutamine and applied onto cells for 1, 6, 12, and 24 hours. Cell culture experiments were repeated 3 times.

Nitrite assay. CM were assayed for nitrite by the Griess reagent (Ignarro et al. 1993) with NaNO₂ as a standard, and untreated media as a blank control. Assays used 96-well plates, with 50 ul of CM in duplicate and 50 ul Griess reagent for 10 minutes in the dark at room temperature, prior to reading at 550nm.

Western blots. Brain regions (OE, OB, cerebral cortex, cerebellum) were homogenized by a motor driven pestle on ice in 1x RIPA buffer (Millipore) supplemented with 1mM PMSF, 1mM Na₃VO₂, 10 mM NaF, phosphatase inhibitor cocktails (Sigma), and Roche Complete Mini EDTA-free Protease Inhibitor Cocktail Tablet (Roche). Homogenates were centrifuged 10,000 g

x 10 min/4°C; supernatants were analyzed by Western blots with 20 µg of total protein on Novex NuPAGE 4-12% Bis-Tris protein gels (Thermo Scientific). Membranes were washed with phosphate buffered saline with 0.05% tween-20 (PBST), then blocked with 5% milk/PBST or 5% BSA/PBST for 1 hour at room temperature, followed by overnight incubation with primary antibodies at 4°C: anti-TNFα (1:250, mouse; R&D Systems), anti-3-nitrotyrosine (1:1000, rabbit; Millipore), anti-4-hydroxynonenal (1:250, mouse; R&D Systems), anti-OMP (1:400, goat; Santa Cruz), anti-cleaved caspase 3 (1:1000, rabbit; Cell Signaling), anti-caspase 3 (1:1000, rabbit; Cell Signaling), anti-actin (1:10000, mouse; Sigma). HRP (1:10000, goat; Jackson) enhanced chemiluminescence was detected using West Pico Chemiluminescent Substrate (Thermo Scientific). Density of bands was assessed with imageJ.

Immunohistochemistry. Following nPM treatment and euthanasia, heads were de-skinned, fixed in 10% neutral-buffered formalin in 4°C overnight and de-calcified (Shandon's TBD-1 Decalcifier; Thermo Scientific, Waltham, MA), followed by cryoprotection by submersion in a 10-30% sucrose/PBS pH 7.4 gradient. Heads were embedded in OCT compound for cryostat sectioning. For OE sections, brain tissue was removed posterior to the olfactory bulb (OB). Tissue sections (18 µm) on glass slides were permeablized with 1% NP-40/PBS and blocked with 5% BSA. Primary antibodies were added at room temperature overnight for markers of olfactory sensory neurons (OMP - 1:100, goat; Santa Cruz, and NeuN - 1:100, mouse; Millipore), astrocytes (GFAP - 1:400, mouse; Sigma), microglia (Iba1 - 1:200, rabbit; Wako), and oxidative stress (4-HNE - 1:100, rabbit; Millipore, and 3-NT - 1:100, rabbit; Abcam). Immunofluorescence was visualized using Alexa Fluor 488 and 594 antibodies (1:400, goat; Molecular Probes), DAPI (Vector Labs), and HRP (1:400, goat; Jackson) + DAB.

Image Analysis. Images loaded onto ImageJ were converted into 8-bit, then stringently thresholded prior to particle and density analysis. Approximately 12 images were taken for each mouse OB and OE per stain. For microglia, only cells larger than 20 pixels² were considered for analysis. Morphology was determined based on number of visible primary processes (30 per OB for 8 animals). Data was normalized to the pixel area of the tissue when appropriate.

Quantitative Polymerase Chain Reaction (qPCR). Total cellular RNA was extracted by TriReagent (Sigma) and 1-bromo-3-chloropropane (Sigma). cDNA was reverse transcribed (Superscript III kit; Invitrogen) from 2 µg RNA; qPCR used appropriate primers for mouse or rat (Valuegene, San Diego, CA). For primer sequences, see Supplemental Material Table S1. Data were normalized to GAPDH and quantified as delta-delta-CT (cycle threshold).

Statistical Analysis. Statistical analyses used Prism Version 6 (Graph Pad, La Jolla, CA). One-tailed t-test were used to test single comparisons regarding inflammatory responses that have been documented in the literature (Morgan et al. 2011; Cheng et al. 2016). Two-tailed t-tests were used to test single comparisons regarding 4-HNE, 3-NT, nitrite and neuronal OMP. Multiple comparisons used ANOVA with Tukey post-test for adjustments. Data were plotted as mean ± SE. Threshold significance level of alpha = 0.05.

Results

Inhaled nPM rapidly induced oxidative stress in olfactory gateways. Cell types in brain that responded to nPM in vivo (Morgan et al. 2011; Levesque et al. 2011a; Win-shwe et al. 2015) were identified immunohistochemically in olfactory epithelium (OE) and olfactory bulb (OB)

(Fig. 1A). Olfactory sensory neurons (OSN) line the nasal cavity, with dendrites projecting towards the external environment away from the lamina propria (Fig. 1B). Iba1-immunopositive macrophages localize primarily in the lamina propria of the OE, with scattered presence in the OSN layer. Astrocytic GFAP was not detectable in the OSN layer, but showed diffuse staining in the lamina propria without definitive astrocytic cell bodies, (Fig. 1B). In contrast, GFAP in the OB showed robust staining of astrocytes with classical morphology. Also note the Iba1-positive microglia in the OB glomerular layer, and the strongly stained OMP-positive neuronal axons (Fig. 1C).

To investigate the earliest OE and OB cellular responses to nPM, adult mice were exposed to re-aerosolized nPM for 5 h and euthanized 18 hours later on the next day (see Supplemental Material, Fig. S1). The OE showed 25% increases in the oxidative stress markers 4-hydroxynonenal (4-HNE) and 3-nitrotyrosine (3-NT) (Fig. 2A,B), with a positive correlation (Fig. 2C). The number of Iba1-positive macrophages was increased by 30% in the OE turbinates, but those in the OE septum did not change in quantity or morphology (Fig. 2D,E). In contrast to the OE, the OB did not show increased 4-HNE or 3-NT staining (Fig. 3A, B). However, the number of Iba1-positive microglia in the OB glomerular layer increased by 30%, without change in the adjacent mitral or granule cell layers (Fig. 3C,D). nPM doubled the number of amoeboid microglia (0-1 primary processes), which implies activation (Fig. 3E). Astrocytic GFAP staining did not change in any OB layer (Fig. 3F,G).

nPM exposure of the olfactory epithelium ex vivo. To further investigate the initial reactions of the OE, we developed two models: (I) ex vivo OE organ culture and (II) dissociated OE primary mixed cell cultures. The OE tissue was incubated in CSF media with 12 µg/ml of nPM, a

concentration that induced TNF α in mixed cerebral cortical glia (Morgan et al. 2011, Cheng et al. 2016). After 2 h incubation, RNA responses included 30% increase of CD68, IL-1 α , and TNF α (see Supplemental Material, Fig. S2A).

nPM induced oxidative stress and inflammation in vitro.

The induction of reactive nitrogen species is indicated by increased 3-NT (Fig. 2A,B). Correspondingly, the conditioned media (CM) from ex vivo OE organ culture showed a 50% increase of nitrite after 2 h of nPM (see Fig. S2B). Dissociated OE cultures also showed increased CM nitrite, continuing from 6 h through 24 h (Fig. 4A).

Because the OE primary cell cultures included OSN cell bodies, we examined mixed cortical glia cultures which have negligible neuronal content. During nPM exposure, nitrite in the CM also increased progressively over 24 h (Fig. 4B). iNOS mRNA was rapidly, but transiently induced by 1 h, with subsequent decrease paralleling nitrite level increases. Other nitric oxide synthases, nNOS and eNOS, did not change with nPM, or had unreliably high CT values (see Supplemental Material, Fig. S3), suggesting that iNOS is the major contributor to the nitrite induction. TNF α mRNA showed a slower induction, increasing after 12-24 h (Fig. 4C).

Extended in vivo nPM exposure induced rapid oxidative stress and inflammation in OE and OB. We extended the in vivo time course of nPM response to total exposures of up to 45 h over 3 weeks (see Supplemental Material, Fig. S1). Corresponding to the immunohistochemistry of the OE (Fig. 2), Western blots of OE showed 30% increase in 4-HNE that persisted from 5 to 45 h of total nPM exposure (Fig. 5A). 3-NT also showed a trend for increase at 5 h, and was significantly increased by 75% at 45 h (Fig. 5A). The olfactory marker protein (OMP), expressed

only by mature OSNs, was reduced by 25% at 45 h of nPM (Fig. 5A). The decrease of OMP varied inversely with levels of cleaved caspase-3, a marker of apoptosis (Fig. 5B). As an indirect measurement of cleaved caspase-3 activity, PARP1 also increased at 45 h in the OE (Fig. 5B). TNF α responded more slowly: the only significant changes were in TNF α mRNA (+75%) at 20 h and in TNF α protein (+60%) at 45 h (Fig. 5C). IL-1 α mRNA fluctuated, with possible transient increase at 20h (not shown). There were no responses of the microglial marker CD68 (Fig. 5C).

The OB showed similarly modest inflammatory and oxidative stress responses to extended nPM exposure (see Supplemental Material, Fig. S4). TNF α mRNA, but not protein, showed a transient increase at 20 h of exposure, while TNF α protein was only increased at 45 h. CD68 mRNA was more consistently increased at 20 h and 45 h (see Fig. S4A). 4-HNE, unlike in the OE, and 3-NT increased in the OB only at 45 h (see Fig. S4B). The olfactory marker protein (OMP) of the olfactory nerve projections did not respond at any time (not shown).

Down-stream responses of cerebral cortex and cerebellum. We assayed the cerebral cortex and cerebellum for comparison with the OE and OB. TNF α mRNA increased 50% in cortex and 70% in cerebellum at 45 h (Fig. 6A, B, D). In parallel to mRNA, TNF α protein increased 50% in cortex and 30% in cerebellum at 45 h (Fig. 6A, B). Cerebellar CD68 mRNA was increased 50% at 20 h and 45 h, but cortex CD68 did not respond (Fig. 6A, B). 3-NT (not shown) and 4-HNE (Fig. 6C) did not change in either region. For comparison with 150 h total exposure over 10 weeks (Morgan et al. 2011), Fig. 6D shows combined data for cerebral cortex CD68 and TNF α mRNA.

Discussion

To our knowledge, these are the first data on the acute cell responses of the nasal olfactory epithelium (OE) to air pollution PM and the first time course of spatial responses of any air pollutant from nose to brain regions. These experiments exposed rodent neural tissues to nPM, a nano-sized subfraction of PM_{2.5} which is enriched in water soluble organic compounds. The *in vivo*, *ex vivo*, and *in vitro* models of the OE showed rapid increase of oxidative stress by 24 h of nPM, with increased tissue levels of 4-HNE, 3-NT, and TNF α (Fig. 2, 4, 5, S2).

We anticipated that the OB would also show rapid responses, because olfactory neurons of the OE axonally transmitted nano-scale gold PM into the olfactory bulb (OB) (De Lorenzo 1970) and because inhaled nano-scale PM of ¹⁴C-graphite and of intranasal Mn were rapidly accumulated in the OB (Oberdörster et al. 2004; Elder et al 2006). However, the OB had smaller increases of 4-HNE and 3-NT and slower responses of TNF α until later in the series of exposures, as did cerebral cortex and cerebellum (see Fig. S4, 6). Only at 45 h of total exposure to nPM during 3 weeks did cerebral cortex TNF α mRNA approach the levels from 150 h of nPM exposure over 10 weeks in our initial study (Morgan et al. 2011). These delayed responses suggest contributions from systemic responses to nPM that may interact with the direct olfactory nerve pathway from nose to brain. We also consider a neuronal degenerative response of the OE that differed from downstream brain regions.

The olfactory sensory neurons (OSN) that line the OE are the only neurons in the respiratory tract that are directly exposed to the external environment, thereby the first neuronal responders to inhaled air pollutants. Early increases of 4-HNE and 3-NT after a 5 h exposure were histochemically localized to the nasal epithelial mucosa, concurrent with increased numbers of macrophages (Iba1-positive) in the turbinate zone (Fig. 2). However, TNF α increases were

delayed in the OE until 20-45 h, as was a neuronal degenerative response in the 25% reduction of the olfactory neuron marker protein OMP with reciprocal increase of cleaved caspase-3 (Fig. 5).

OB responses were more modest and delayed than in the OE. While 4-HNE and 3-NT increased by 45 h (see Fig. S4), we did not detect any change in neuronal OMP, unlike the OE. Furthermore, the downstream cerebral cortex or cerebellum did not show increased 4-HNE or 3-NT at any time, while TNF α was only increased at 45 h (Fig. 6). We anticipate that longer exposure to nPM would increase 3-NT in the brain, as observed for 80 h cumulative exposure to diesel exhaust that increased whole brain 3-NT by >100% (Levesque et al. 2011a). Because the cerebral cortex and cerebellum are at least 2 synapses from the OSN (Kronenbueger et al. 2010), it is notable that their TNF α induction was similar in size to TNF α increases in the OB and OE. The relatively larger size of these nasally distant brain regions raises an important question: one might expect that transynaptically transported nPM would be diluted in some proportion to the brain mass, from the OB (25 mg wet weight) to the cerebral cortex (200 mg) and the more remote cerebellum (70 mg), yet the TNF α induction is similar. Could systemic mechanisms be involved?

Several lines of evidence support the role of systemic import of particulate material or of pro-inflammatory factors. In the highly respected study of Oberdörster et al. 2004, a single exposure to inhaled nanoscale ¹⁴C-graphite caused brain levels of ¹⁴C that were as high or higher in cerebellum as in the OB after 5 days. These authors discussed possible "...translocation across the blood-brain barrier in certain regions". A blood-born source of the persisting ¹⁴C elevations in cerebellum and cerebrum would be consistent with the large residual ¹⁴C pool of the lung. Further evidence for a lung-to-brain axis in air pollution comes from brain responses to intra-tracheal installation of a PM10 air pollutant fraction, which induced the oxidatively sensitive

gene HO-1 by >100% in both whole brain and lung (Farina et al. 2013). Systemic transmission of particles or inflammatory factors is also consistent with effects on fetal brain from intra-tracheal DEP (Bolton et al. 2014). Moreover, inhaled vehicular emissions increased permeability of the blood-brain barrier (BBB) in mice, while serum from pollution exposed mice increased BBB permeability in an in vitro model (Oppenheim et al. 2013) and altered vasorelaxation with CD36 dependence (Robertson et al. 2013). Lastly, we note that increased circulating cytokines from respiratory tract inflammation can cross the BBB and evoke neuroinflammatory responses (Peters et al. 2006; Erickson et al. 2012). Thus, systemic effects of air pollution warrant further study in conjunction with the established direct nose-brain pathway. We anticipate complex transitions of pathway specific mechanisms during prolonged exposures.

The induction of TNF α , 4-HNE, and 3-NT implicate oxidative and inflammatory mechanisms during in vivo exposure. The rapid increase in 4-HNE and 3-NT in OE was associated with nitrosative stress with several in vitro models. Ex vivo intact OE was incubated with nPM under conditions based on prior studies of hippocampal slices, in which nPM increased nitric oxide (NO) and S-nitrosylation (Davis et al. 2013). The ex vivo and primary OE cultures showed increased nitrite in response to nPM (see Fig. S2, 4). Mixed glia from cerebral cortex also responded to nPM with induced nitrite and iNOS. The ex vivo OE also showed induction of cytokines (IL-1 α , TNF α) and macrophage activation (CD68). The neonatal rat OE had similar ex vivo responses (Cheng et al. 2016). These changes parallel the in vivo rapid inflammatory responses to nPM inhalation, which include increased Iba1-positive macrophages in the OE turbinate layer and in the OB glomerular layer (Fig. 2, 3).

The inflammatory changes seen in the OE and brain may be propagated by macrophage/microglial activation in response to oxidative stress induced by nPM. Macrophage

scavenger receptors, including CD36, can be activated by 4-HNE (Ishii et al. 2004; Stewart et al. 2010). Additionally, modified adducts of HNE by glutathione may activate NF-KB (Ramana et al. 2006) as well as induce TNF α . These oxidative markers, 4-HNE and 3-NT, are implicated in the pathogenesis of Alzheimer's disease (AD) and other neurodegenerative disorders (Shringarpure et al. 2000; Butterfield et al. 2007; Dalleau et al. 2013).

There are notable variations of OB responses between exposure models (Levesque et al. 2011b; Gerlofs-Nijland et al. 2010; Guerra et al. 2013). The lack of, or attenuated, OB responses in longer exposures with baseline return of TNF α mRNA by 45 h in our data suggests compensatory OB mechanisms. This warrants more attention: Ong et al. 2015 showed that a single 4 h exposure over 1 day to 0.5 ppm ozone, a gaseous pollutant absent from nPM, transiently induced TNF α mRNA by 70% in the nasal mucosa, with return to control levels by 4 d of exposure (Wagner et al. 2002; Ong et al. 2015). Moreover, there was rapid infiltration of neutrophils into the nasal mucosa within 2 h after initial exposure. In our model, the lack of TNF α , IL-1 β , CD68 mRNA responses in OE and OB by 1 d of nPM inhalation suggests that ozone-mediated toxicity in nasal mucosa occurs more rapidly through different mechanisms.

Neurodegenerative changes in olfactory neurons arose much later in the OE, measured by a reduction in levels of the OSN specific protein OMP with inverse proportion to the apoptosis marker, cleaved caspase-3 (Fig. 5A, B). The induction of TNF α in the OE may interfere with OSN regeneration (Turner et al. 2010). The OSNs, being exposed to inhaled environmental toxins, are continuously regenerated in conjunction with apoptosis to maintain functionality (Holcomb et al. 1996). Moreover, extended chronic exposure to ultrafine PM also induced apoptosis (Win-shwe et al. 2011). These observations are consistent with studies on domestic dogs from a highly polluted city which showed disrupted OSN and sustentacular cell layers, with

an overall thinning of the OE (Garcidueña et al. 2003). Relevant to humans, late onset olfactory dysfunction is a risk factor for AD (Devanand et al. 2000; Arnold et al. 2010).

In vitro models of OE may help identify specific air pollution component cytotoxic activities. For example, we do not know the role of free radicals that persist in nPM at least 30 days after initial collection and subsequent re-aerosolization (Morgan et al. 2011). Further fractionation of nPM could also resolve the activities of particular water-insoluble organic compounds.

Conclusions

These data support the hypothesis that inhaled nPM rapidly causes oxidative stress in the olfactory epithelium, with delayed inflammatory and neurodegenerative responses that include increased apoptosis of olfactory neurons. Although the olfactory bulb receives direct input from olfactory neurons, its inflammatory and oxidative stress responses were delayed. The cerebral cortex and cerebellum also responded with slower increase of TNF α , but did not show increased nitrosylated proteins or oxidized lipids at any time. These delayed brain responses suggest that inhaled nPM in the olfactory epithelium and bulb contribute to neurodegenerative effects of air pollution particulates. Systemic factors also merit further consideration in brain responses to air pollution. We hypothesize that the brain-wide increase of TNF α and other cytokines from air pollution exposure contributes to the cognitive deficits epidemiologically associated with air pollutants. TNF α has well-defined links to glutamatergic functions in the hippocampus and cerebral cortex (Beattie et al. 2002; Santello and Volterra 2012) that are critical to learning and memory.

References

- Ailshire JA, Crimmins EM. 2014. Fine particulate matter air pollution and cognitive function among older US adults. *Am J Epidemiol* 180:359-366.
- Arnold SE, Lee EB, Moberg PJ, Stutzbach L, Kazi H, Han LY, et al. 2010. Olfactory Epithelium Amyloid- β and PHFtau Pathology in Alzheimer's Disease. *Ann Neurol* 67:462-469.
- Beattie EC, Stellwagen D, Morishita W, Bresnahan JC, Ha BK, Von Zastrow M, et al. 2002. Control of synaptic strength by glial TNFalpha. *Science* 295:2282-2285.
- Block ML, Elder A, Auten RL, Bilbo SD, Chen H, Chen JC, et al. 2012. The outdoor air pollution and brain health workshop. *Neurotoxicology* 33:972-984.
- Bolton JL, Auten RL, Bilbo SD. 2014. Prenatal air pollution exposure induces sexually dimorphic fetal programming of metabolic and neuroinflammatory outcomes in adult offspring. *Brain Behav Immun* 37:30-44.
- Butterfield DA, Reed TT, Perluigi M, Marco CD, Coccia R, Keller JN, et al. 2007. Elevated levels of 3-nitrotyrosine in brain from subjects with amnesic mild cognitive impairment: implications for the role of nitration in the progression of Alzheimer's disease. *Brain Res* 1148:243-248.
- Butterfield DA, Reed T, Sultana R. 2011. Roles of 3-nitrotyrosine- and 4-hydroxynonenal-modified brain proteins in the progression and pathogenesis of Alzheimer's disease. *Free Radic Res* 45:59-72.
- Calderón-Garcidueñas L, Engle R, Mora-Tiscareño A, Styner M, Gómez-Garza G, Zhu H, et al. 2011. Exposure to severe urban air pollution influences cognitive outcomes, brain volume and systemic inflammation in clinically healthy children. *Brain Cognition* 77:345-355.
- Calderón-Garcidueñas L, Maronpot R, Torres-Jardon R, Henríquez-Roldán C, Schoonhoven R, Acuña-Ayala H, et al. 2003. DNA damage in nasal and brain tissues of canines exposed to air

pollutants is associated with evidence of chronic brain inflammation and neurodegeneration. *Toxicologic Path* 31:524-538.

Campbell A, Oldham M, Becaria A, Bondy SC, Meacher D, Sioutas C, et al. 2005. Particulate matter in polluted air may increase biomarkers of inflammation in mouse brain. *Neurotoxicology* 26:133-140.

Chen JC, Schwartz J. 2009. Neurobehavioral effects of ambient air pollution on cognitive performance in US adults. *Neurotoxicology* 30:231-239.

Chen JC, Wang X, Wellenius G, Serre M, Driscoll I, Casanova R, et al. 2015. Ambient air pollution and neurotoxicity on brain structure: evidence from Women's Health Initiative Memory Study. *Ann Neurol* 78:466-476.

Cheng H, Davis DA, Hasheminassab S, Sioutas C, Morgan TE, Finch CE. 2016. Urban traffic-derived nanoparticulate matter reduces neurite outgrowth via TNF α in vitro. *J Neuroinflammation*. In press.

Dalleau S, Baradat M, Guéraud F, Huc L. 2013. Cell death and diseases related to oxidative stress: 4-hydroxynonenal (HNE) in the balance. *Cell Death Differ* 20:1615-1630.

Davis DA, Akopian G, Walsh JP, Sioutas C, Morgan TE, Finch CE. 2013. Urban air pollutants reduce synaptic function of CA1 neurons via an NMDA/N O pathway. *J Neurochem* 127:509-519.

DeLorenzo AJ. 1970. The olfactory neuron and the blood-brain barrier. In: *Taste and Smell in Vertebrates*. London: J&A Churchill, 151–176.

Devanand DP, Michaels-Marston KS, Liu X, Pelton GH, Padilla M, Marder K, et al. 2000. Olfactory deficits in patients with mild cognitive impairment predict Alzheimer's disease at follow-up. *Am J Psychiatry* 157:1399-1405.

Elder A, Gelein R, Silva V, Feikert T, Opanashuk L, Carter J, et al. 2006. Translocation of inhaled ultrafine manganese oxide particles to the central nervous system. *Environ Health Perspect* 114:1172-1178.

Erickson MA, Dohi K, Banks WA. 2012. Neuroinflammation: a common pathway in CNS diseases as mediated at the blood-brain barrier. *Neuroimmunomodulation* 19:121-130.

Farina F, Sancini G, Battaglia C, Tinaglia V, Mantecca P, Camatini M, et al. 2013. Milano summer particulate matter (PM10) triggers lung inflammation and extra pulmonary adverse events in mice. *PLoS One* 8:e56636; doi:10.1371/journal.pone.0056636.

Gatto NM, Henderson VW, Hodis HN, St. John JA, Lurmann F, Chen JC, et al. 2014. Components of air pollution and cognitive function in middle-aged and older adults in Los Angeles. *Neurotoxicology* 40:1-7.

Gerlofs-Nijland ME, Totlandsdal AI, Kiliç E, Boere AJ, Fokkens PH, Leseman DL, et al. 2010. Pulmonary and cardiovascular effects of traffic-related particulate matter: 4-week exposure of rats to roadside and diesel engine exhaust particles. *Inhal Toxicol* 22:1162-1173.

Gillespie P, Tajuba J, Lippmann M, Chen LC, Veronesi B. 2013. Particulate matter neurotoxicity in culture is size-dependent. *Neurotoxicology* 36:112-117.

Guerra R, Vera-Aguilar E, Uribe-Ramirez M, Gookin G, Camacho J, Osornio-Vargas AR, et al. 2013. Exposure to inhaled particulate matter activates early markers of oxidative stress, inflammation and unfolded protein response in rat striatum. *Toxicol Lett* 222:146-154.

Hasheminassab S, Daher N, Schauer JJ, Sioutas C. 2013. Source apportionment and organic compound characterization of ambient ultrafine particulate matter (PM) in the Los Angeles Basin. *Atmos Environ* 79:529–539.

Holcomb DJ, Graham S, Calof AL. 1996. Neuronal homeostasis in mammalian olfactory epithelium: a review. *Am J Rhinol* 10:125-134.

Ignarro LJ, Fukuto JM, Griscavage JM, Rogers NE, Byrns RE. 1993. Oxidation of nitric oxide in aqueous solution to nitrite but not nitrate: comparison with enzymatically formed nitric oxide from L-arginine. *Proc Natl Acad Sci U S A.* 90:8103–8107.

Ishii T, Itoh K, Ruiz E, Leake DS, Unoki H, Yamamoto M, et al. 2004. Role of Nrf2 in the regulation of CD36 and stress protein expression in murine macrophages: activation by oxidatively modified LDL and 4-Hydroxynonenal. *Circ Res* 94: 609-616.

Kraft AD, Harry JG. 2011. Features of microglia and neuroinflammation relevant to environmental exposure and neurotoxicity. *Int J Environ Res Public Health* 8: 2980-3018.

Kronenbueger M, Zobel S, Ilgner J, Finkelmeyer A, Reinacher P, Coenen VA, et al. 2010. Effects of deep brain stimulation of the cerebellothalamic pathways on the sense of smell. *Exp Neurol* 222:144-152.

Li N, Sioutas C, Cho A, Schmitz D, Misra C, Sempf J, et al. 2002. Ultrafine particulate pollutants induce oxidative stress and mitochondrial damage. *Environ Health Perspect* 111:455-460.

Levesque S, Taetzsch T, Lull ME, Kodavanti U, Stadler K, Wagner A, et al. 2011a. Diesel exhaust activates and primes microglia: air pollution, neuroinflammation, and regulation of dopaminergic neurotoxicity. *Environ Health Perspect* 119:1149-1155.

Levesque S, Surace MJ, McDonald J, Block ML. 2011b. Air pollution & the brain: subchronic diesel exhaust exposure causes neuroinflammation and elevates early markers of neurodegenerative disease." *J Neuroinflammation* 8:105; doi:10.1186/1742-2094-8-105.

Misra C, Kim S, Shen S, Sioutas C. 2002. A high flow rate, very low pressure drop impactor for inertial separation of ultrafine from accumulation mode particles. *J Aerosol Sci* 33:735-752.

Morgan TE, Davis DD, Iwata N, Tanner JM, Snyder D, Ning Z, et al. 2011. Glutamatergic neurons in rodent models respond to nanoscale particulate urban air pollutants in vivo and in vitro. *Env Health Perspect* 119:1003-1009.

Oberdörster G, Sharp Z, Atudorei V, Elder A, Gelein R, Kreyling W, et al. 2004. Translocation of inhaled ultrafine particles to the brain. *Inhal Toxicol* 16:437-445.

Ong CB, Kumagai K, Brooks PT, Brandenberger C, Lewandowski RP, Jackson-Humbles DN, et al. 2015. Ozone-induced Type 2 immunity in nasal airways: development and lymphoid cell dependence in mice. *Am J Respir Cell Mol Biol*. Epub ahead of print.

Oppenheim HA, Lucero J, Guyot AC, Herbert LM, McDonald JD, Mabondzo A, et al. 2013. Exposure to vehicle emissions results in altered blood brain barrier permeability and expression of matrix metalloproteinases and tight junction proteins in mice. *Part Fibre Toxicol* 10:62.

Peters A, Veronesi B, Calderón-Garcidueñas L, Gehr P, Chen LC, Geiser M, et al. 2006. Translocation and potential neurological effects of fine and ultrafine particles a critical update. *Part Fibre Toxicol* 3:13; doi:10.1186/1743-8977-3-13.

Ramana KV, Fadhil AA, Tammali R, Reddy BMA, Chopra AK, and Srivastava SD. 2006. Aldose Reductase Mediates the Lipopolysaccharide-induced Release of Inflammatory Mediators in RAW264.7 Murine Macrophages. *J Biol Chem* 281:33019-3029.

Robertson S, Colombo ES, Lucas SN, Hall PR, Febbraio M, Paffett ML, et al. 2013. CD36 mediates endothelial dysfunction downstream of circulating factors induced by O₃ exposure. *Toxicol Sci* 134:304-311.

Rozovsky I, Finch CE, Morgan TE. 1998. Age-related activation of microglia and astrocytes: in vitro studies show persistent phenotypes of aging, increased proliferation, and resistance to down-regulation. *Neurobiol Aging* 19:97-103.

Saffari A, Daher N, Shafer MM, Schauer JJ, Sioutas C. 2013. Seasonal and spatial variation of trace elements and metals in quasi-ultrafine (PM_{0.25}) particles in the Los Angeles metropolitan area and characterization of their sources. *Environ Pollut* 181:14–23.

Santello M, Volterra A. 2012. TNF α in synaptic function: switching gears. *Trends Neurosci* 35:638-647.

Shringarpure R, Grune T, Sitte N, Davies KJ. 2000. 4-Hydroxynonenal-modified amyloid-beta peptide inhibits the proteasome: possible importance in Alzheimer's disease. *Cell Mol Life Sci* 57:1802–1809.

Stewart CR, Stuart LM, Wilkinson K, van Gils JM, Deng J, Halle A, et al. 2010. CD36 ligands promote sterile inflammation through assembly of a Toll-like receptor 4 and 6 heterodimer. Nat Immunol 11:155-161.

Tonne C, Elbaz A, Beevers S, Singh-Manoux A. 2014. Traffic-related air pollution in relation to cognitive function in older adults. *Epidemiology* 25:674-681.

Turner JH, Liang KL, May L, Lane AP. 2010. Tumor Necrosis Factor-alpha inhibits olfactory regeneration in a transgenic model of chronic rhinosinusitis-associated olfactory loss. *Am J Rhinol* 24:336-340.

Wang D, Pakbin P, Saffari A, Shafer MM, Schauer JJ, Sioutas C. 2013. Development and evaluation of a high-volume aerosol-into-liquid collector for fine and ultrafine particulate matter. *Aerosol Sci Tech* 47:1226-1238.

Wagner JG, Hotchkiss JA, Harkema JR. 2002. Enhancement of nasal inflammatory and epithelial responses after ozone and allergen coexposure in Brown Norway rats. *Toxicol Sci* 67:284-294.

Win-Shwe TT, Fujimaki H. 2011. Nanoparticles and neurotoxicity. *Int J Mol Sci* 12:6267-6280.

Win-Shwe TT, Yamamoto S, Ahmed S, Kakeyama M, Kobayashi T, Fujimaki H. 2006. Brain cytokine and chemokine mRNA expression in mice induced by intranasal instillation with ultrafine carbon black. *Toxicol Lett* 163:153-160.

Win-Shwe TT, Kyi-Tha-Thu C, Moe Y, Maekawa F, Yanagisawa R, Furuyama A, et al. 2015. Nano-sized secondary organic aerosol of diesel engine exhaust origin impairs olfactory-based spatial learning performance in preweaning mice. *Nanomaterials* 5:1147-1162.

Figure Legends

Figure 1. Model of olfactory gateway to brain. (A) Schema, dorsal transverse plane, of the olfactory epithelium (OE) and olfactory bulb (OB). The outlined boxes identify displayed regions for OE and OB; red dashed line represents an OSN and olfactory axon projection to OB. (B) Olfactory epithelium lining the ethmoturbinate space contains olfactory sensory neurons (OSNs) and Iba1-positive macrophages; Glial fibrillary acidic protein (GFAP) shows diffuse staining in lamina propria, but was not detected above background in the OSN layer. Nuclei were identified with DAPI. (C) The OB contains OSN projections in the glomerular layer (glom. layer), astrocytes, and microglia. Olfactory marker protein (OMP) staining is shown at lower magnification for clarity. *Scale bar* = 50 μm .

Figure 2. Acute in vivo nPM exposure induced oxidative stress and inflammation in olfactory epithelium (OE): immunohistochemistry. (A) Representative immunostaining of 4-hydroxynonenal (4-HNE) and 3-nitrotyrosine (3-NT) in OE. (B) 5 h exposure increased 4-HNE and 3-NT staining by 25% in OE vs. controls ($n = 8$ noses/group). *Scale bar* = 100 μm . (C) 4-HNE and 3-NT staining were positively correlated ($r^2 = 0.27$). (D) Iba1-positive macrophages. (E) Macrophage numbers increased in the OE turbinates, but not in the OE septum (left: CTL, right: nPM). *Scale bar* = 50 μm . (*; $p < 0.05$, **; $p < 0.01$; t-test).

Figure 3. Acute in vivo nPM exposure responses in olfactory bulb (OB): immunohistochemistry. (A) Immunostaining of 4-HNE and 3-NT in OB. (B) 4-HNE and 3-NT did not change significantly ($n = 8$). *Scale bar* = 100 μm . (C) Representative immunostaining of Iba1-positive macrophages. (D) nPM exposure increased the number of microglia in the OB glomerular layer by 30%, but not in mitral or granule cell layers. (*; $p < 0.05$; t-test). (E) Representative images of ramified vs amoeboid microglia. *Scale bar* = 25 μm . nPM doubled the

percentage of microglia without multiple processes; the total percent of activated microglia did not change. (*; $p < 0.05$; two-way ANOVA). (F) Immunostaining of astrocytes with GFAP. (G) GFAP immunostained area per region was not altered by nPM exposure in any OB layer. *Scale bar* = 50 μm .

Figure 4. In vitro time course exposure to nPM induced oxidative stress and inflammation in primary cultures of rat OE and cerebral cortex mixed glia.

(A) Conditioned media (CM) from dissociated OE cultures with 12 $\mu\text{g/ml}$ nPM showed time-dependent increase of nitrite. (B) Cerebral cortex mixed glial (MxG) cultures with 12 $\mu\text{g/ml}$ nPM transiently induced iNOS mRNA by 160%. Correspondingly, nPM doubled the CM nitrite by 12 h. (C) TNF α mRNA was increased by 125% after 12 h, remaining elevated at 24 h ($n = 6/\text{group/time}$). (*; $p < 0.05$, **; $p < 0.01$, ***; $p < 0.001$; t-test).

Figure 5. nPM in vivo exposure induced oxidative stress and inflammation in the OE.

(A) 4-HNE adducted proteins were increased 30% after 5 h of exposure, and remained elevated at 45 h of exposure. 3-NT adducted proteins were increased 75% after 45 h of exposure. Olfactory marker protein (OMP) was decreased 25% by 45 h of exposure. (B) Cleaved caspase-3 showed a 20% increase by 20 h and 45 h of exposure. OMP varied inversely with cleaved caspase-3 (Spearman correlation, $r = -0.61$). Each data point represents the % change vs controls. Cleaved PARP1, an indirect product of cleaved caspase-3 activity, was increased 60% after 45 h of exposure. (C) TNF α mRNA transiently increased 75% in OE after 20 h of cumulative nPM exposure vs. controls. TNF α protein increased later 60% at 45 h. CD68 did not change ($n = 6$ mice/group/time). (*; $p < 0.05$; t-test).

Figure 6. Extended nPM in vivo exposure induced TNF α in the cerebral cortex and cerebellum.

(A) TNF α mRNA increased 50% in cortex after 45 h of cumulative nPM exposure

vs. controls (n = 6 mice/group/time). TNF α protein increased 50% after 45 h. CD68 mRNA did not change. (B) Cerebellar TNF α mRNA increased 70% after 45 h. TNF α protein increased by 30% after 45 h. CD68 mRNA was increased 50% at 20 h and 45 h. (C) 4-HNE did not change in cerebral cortex or cerebellum. (D) Present data are graphed with prior findings from 150 h nPM exposure, which increased TNF α and CD68 by 50% and 90% respectively (Morgan et al. 2011). (*; p<0.05; t-test).

Figure 1.

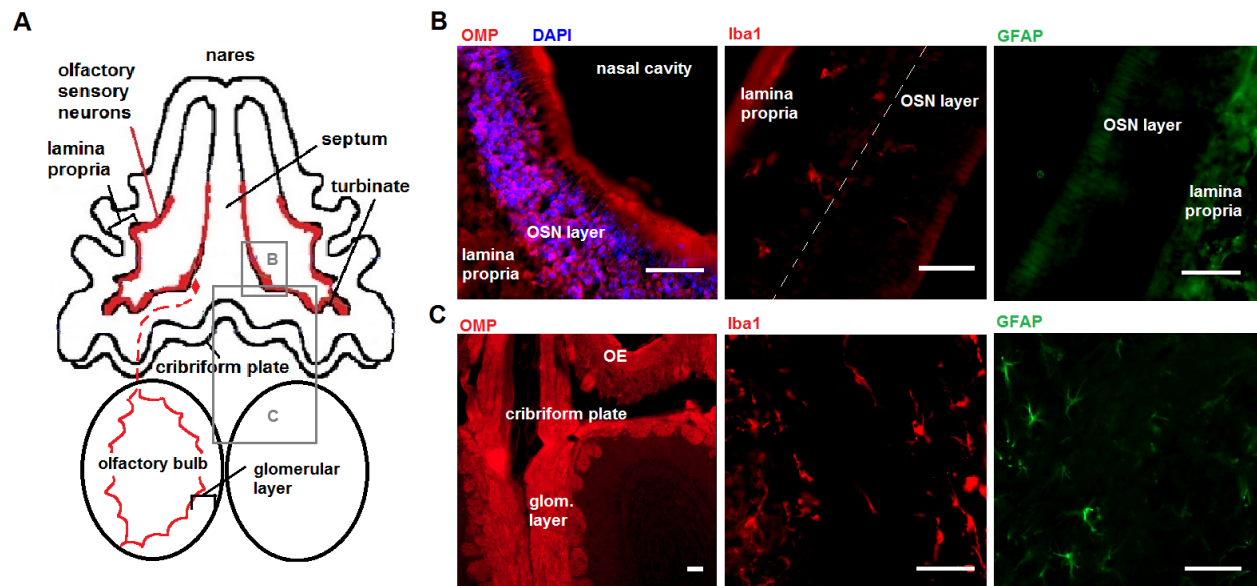


Figure 2.

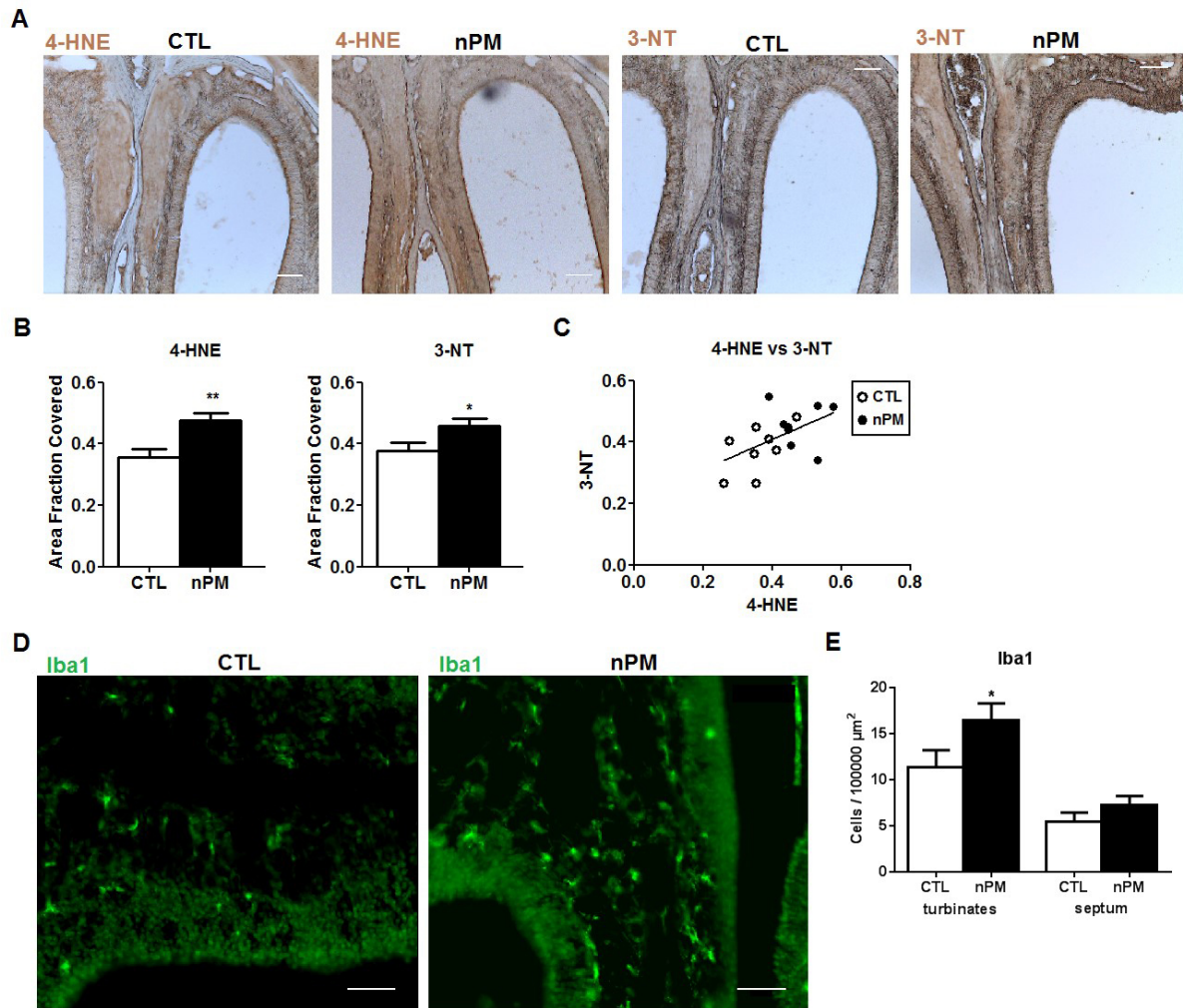


Figure 3.

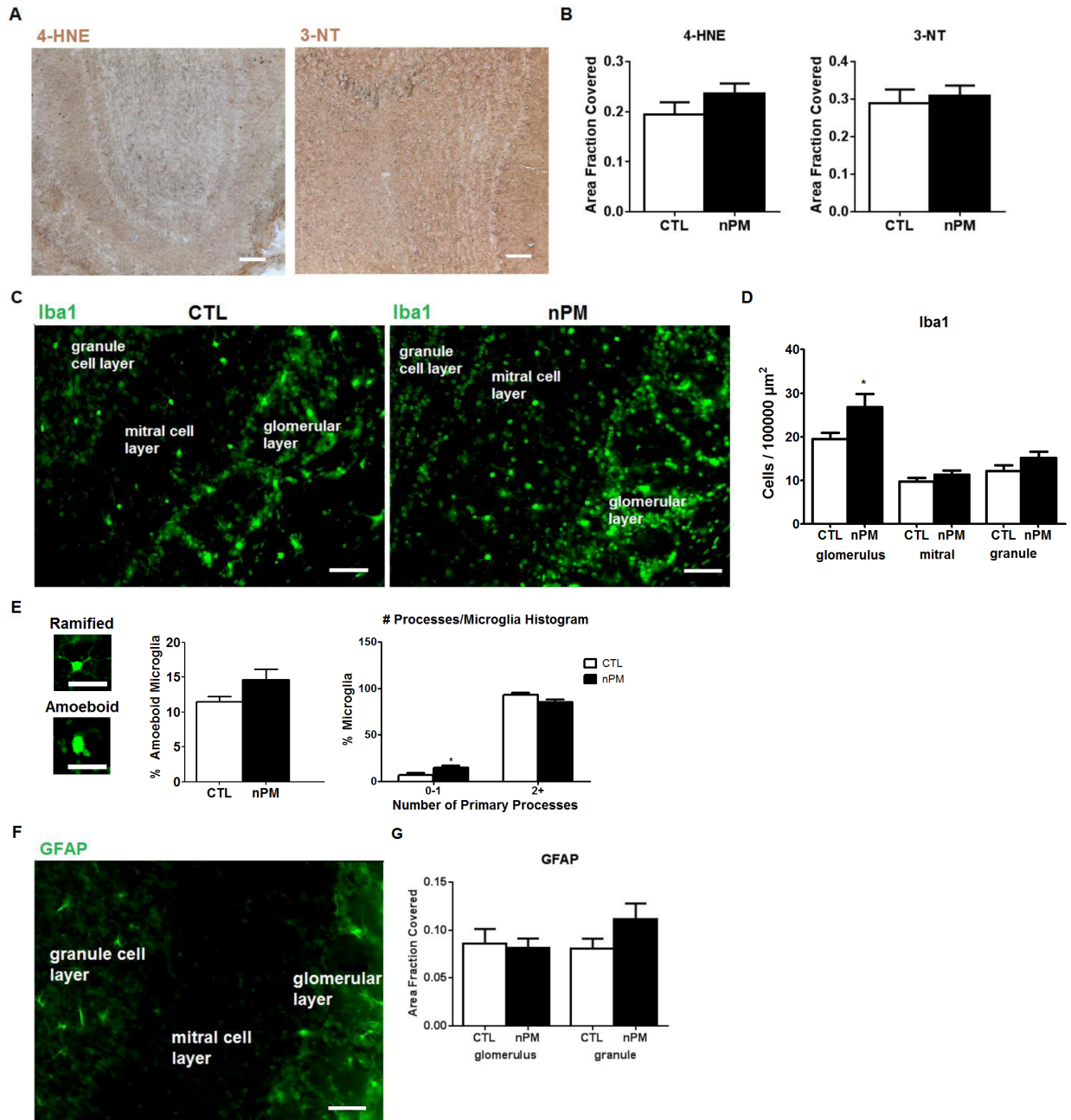


Figure 4.

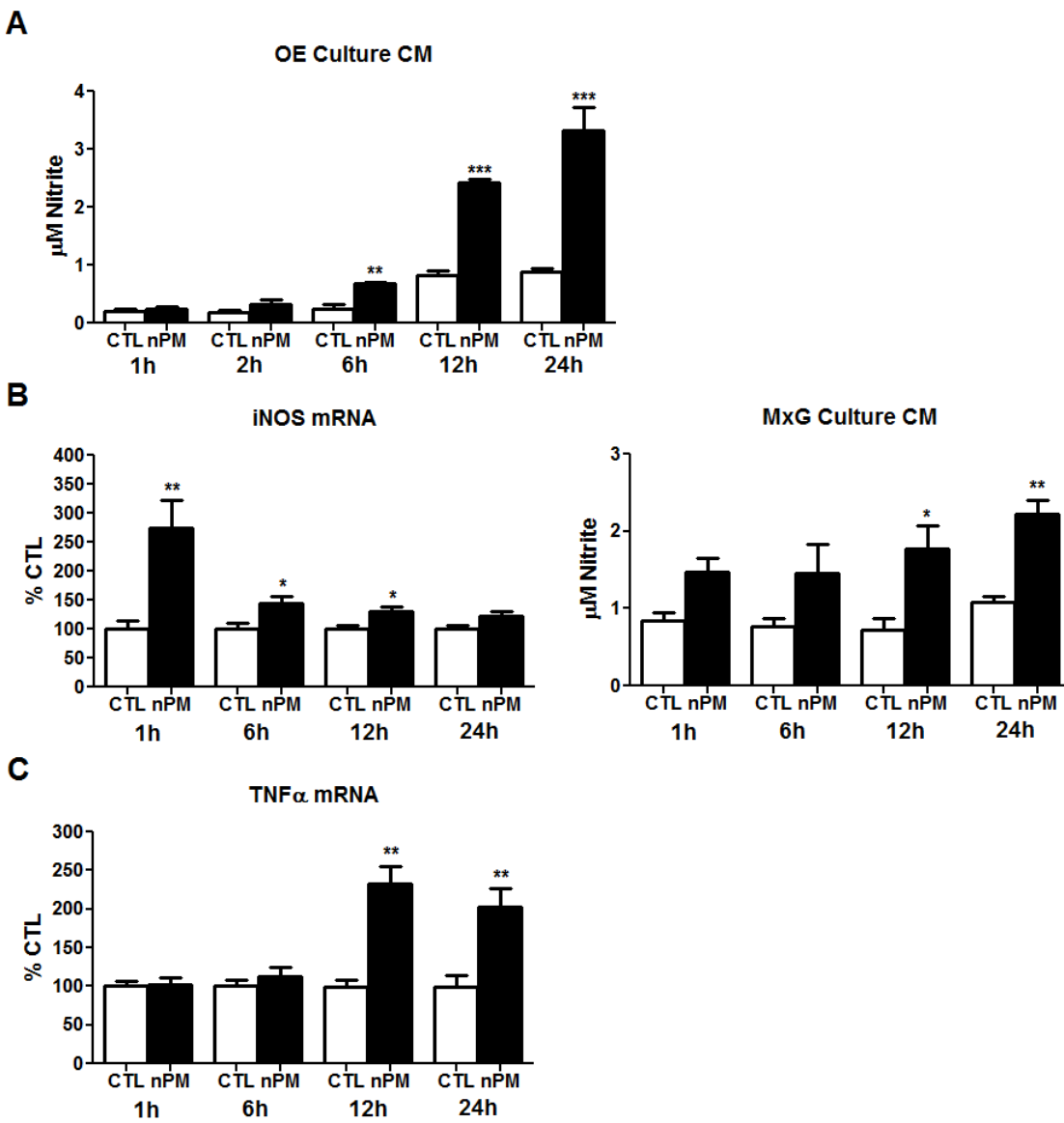


Figure 5.

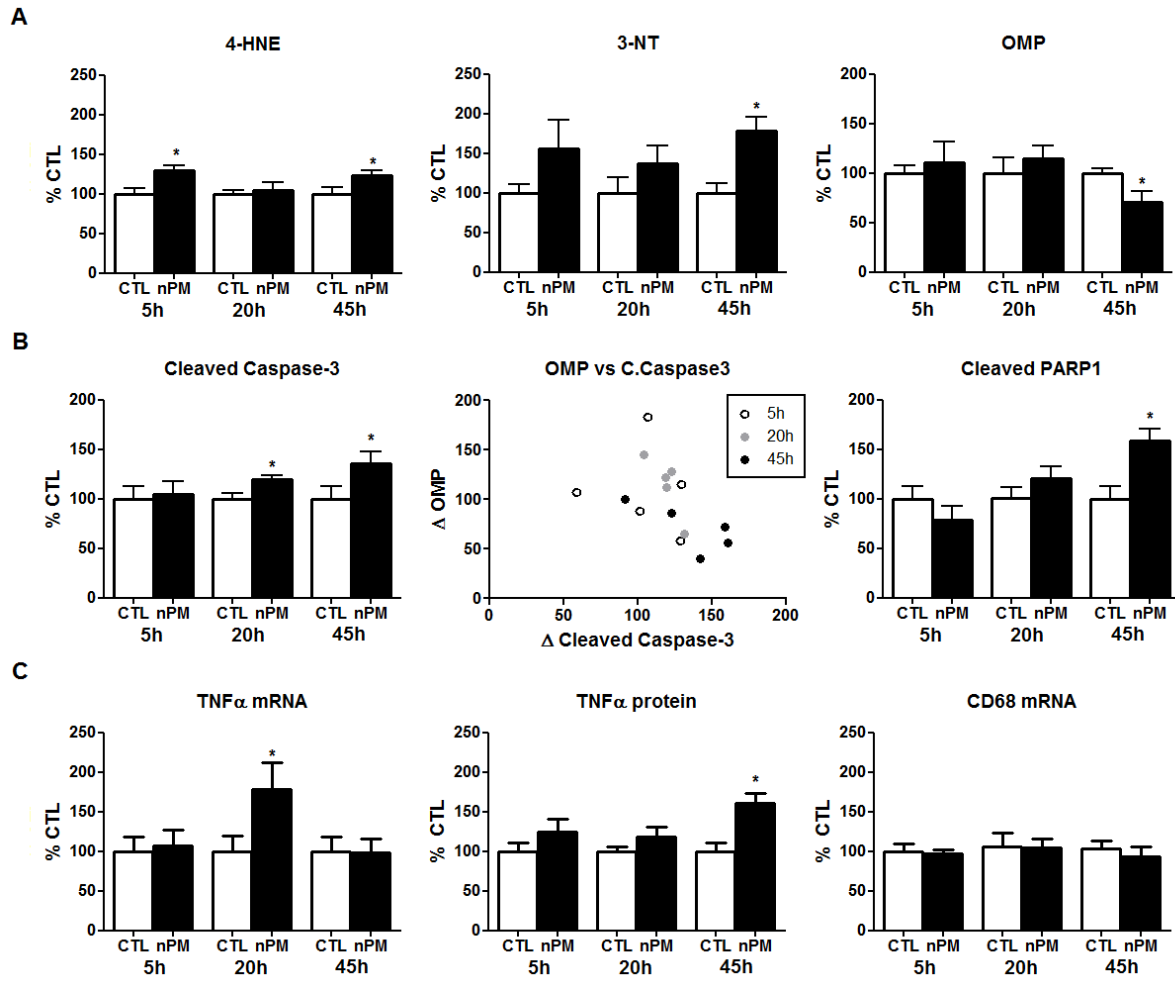


Figure 6.

